Quantum chemical analysis of the bond lengths in f^n and $f^{n-1}d^1$ states of Ce^{3+}, Pr^{3+}, Pa^{4+}, and U^{4+} defects in chloride hosts

Zoila Barandiarán[a] and Luis Seijo
Departamento de Química, C-XIV and Instituto Universitario de Ciencia de Materiales Nicolás Cabrera, Universidad Autónoma de Madrid, 28049 Madrid, Spain

(Received 4 April 2003; accepted 20 May 2003)

It is widely believed that impurity–ligand bond distances in lanthanide (Ln) and actinide (An) doped crystals, are larger in the $f^{n-1}d^1$ energy levels than in the f^n ones. This idea, which was not justified and is probably based on the fact that Ln $5d$ (An $6d$) orbitals have a radial extent much larger than Ln $4f$ (An $5f$) orbitals, has been neither confirmed nor rejected experimentally in spite of the fact that a very large number of absorption/emission spectroscopic studies on f-element doped hosts exist, because the band shapes depend on the square of the bond length offsets between initial and final electronic states. Recent quantum chemical calculations on Ln and An impurities in fluoride and chloride cubic hosts, which considered host embedding, dynamic electron correlation, and relativistic spin–free and spin–orbit coupling effects, have shown that impurity–ligand bond distances are classified in three sets according to their configuration, with the following trend: $R_e[f^{n-1}d(t_{2g})^1] < R_e[f^n] < R_e[f^{n-1}d(e_g)^1]$, in contradiction with the assumed expectations. In this paper we give an interpretation of this, on the basis of a constrained space orbital variation analysis of the chemical bond in states of the f^n, $f^{n-1}d(t_{2g})^1$, and $f^{n-1}d(e_g)^1$ configurations of four model systems: $Cs_2NaYCl_6:Ce^{3+}$, $Cs_2NaYCl_6:Pr^{3+}$, $Cs_2ZrCl_6:Pa^{4+}$, and $Cs_2ZrCl_6:U^{4+}$. The analysis shows that the basic difference between f^n and $f^{n-1}d^1$ configurations regarding bond effects which are responsible for the bond distance is that, in the former, all the open-shell electrons are shielded from the ligands by the $5p$ ($6p$) filled shell and the bond length is determined by closed-shell interactions between the outermost Ln $5p^6$ (An $6p^6$) shell and the ligands, whereas in the latter one electron has crossed the $5p$ ($6p$) barrier and is much more exposed to bonding interactions with the ligands, at the same time that an internal $4f$ ($5f$) hole has been created which induces ligand to Ln (An) charge transfer, all of it resulting in the shown trends. © *2003 American Institute of Physics.* [DOI: 10.1063/1.1590952]

I. INTRODUCTION

The interest in new solid state materials able to produce laser emission or very intense fluorescence in the ultra violet (UV)/vacuum UV spectral regions,[1–5] act as quantum cutters,[6–8] or emit upconverted light,[9–11] has resulted in an increase in the number of spectroscopic studies involving $4f^{n-1}5d^1$ electronic states of lanthanide ion impurities in crystals. Also, the idea that the $5f^{n-1}6d^1$ manifolds of the actinide series could have analogous value and potentiality is leading new research on crystals doped with actinide ions.[12–15] The absorption and emission electronic transition energies observed with high resolution spectroscopies, and their interpretation, are providing much knowledge on the factors governing the energy differences between the f^n manifolds and the higher, partially overlapping $f^{n-1}d^1$ manifolds, and on the energy transfer mechanisms. In clear contrast to this, very little quantitative information is available on the local geometry of the defects around the lanthanide (Ln) and actinide (An) impurities. In principle, extended x-ray absorption fine structure experiments could give bond distances and angles between the impurity and its closest neighbors in the f^n ground state of the defect; however, the local geometry in excited $f^{n-1}d^1$ levels is out of reach for direct measurement. Yet, it is possible to show that the f^n and $f^{n-1}d^1$ manifolds have different nuclear equilibrium configurations and to estimate the absolute value of their shift, out of the analysis of the absorption and emission band shapes. In this respect, it is widely assumed (either explicitely or implicitely) that the bond distances between the lanthanide (actinide) ion and the ligands are larger in the $f^{n-1}d^1$ levels than in the f^n levels (cf. configuration coordinate diagrams in Figs. 2, 3, and 7 of Refs. 4, 13, 16, and 17, respectively, among many examples of this extended assumption). This idea is probably based on the fact that Ln $5d$ (An $6d$) orbitals have a radial extent much larger than Ln $4f$ (An $5f$) orbitals. Only exceptionally, it has been pointed out the possibility of an opposite shift.[18]

The mentioned assumption has been recently contradicted in a series of *ab initio* theoretical studies on the structure and spectroscopy of actinide ion impurities in cubic chloride cristals ($Cs_2ZrCl_6:Pa^{4+}$,[19] $Cs_2ZrCl_6:U^{4+}$,[20] and $Cs_2NaYCl_6:U^{3+}$[21]) conducted in our laboratory. The results of An–Cl equilibrium distances, R_e, have shown that the electronic levels of $(AnCl_6)^{q-}$ embedded clusters can be grouped in three sets according to their bond distances. A

[a]Author to whom correspondence should be addressed; electronic mail: zoila.barandiaran@uam.es

first set is formed by all the states of main configuration $5f^n$, whose bond lengths are only very slightly influenced by the ligand field. Two other sets are formed by the states with main configurations $5f^{n-1}6d(t_{2g})^1$ and $5f^{n-1}6d(e_g)^1$, respectively, with significantly different bond distances resulting from the octahedral ligand field effect on the molecular orbitals with main character An $6d$. The trend has been found to be[19–21]

$$R_e[5f^{n-1}6d(t_{2g})^1] < R_e[5f^n] < R_e[5f^{n-1}6d(e_g)^1].$$

The calculated offsets between $5f^n$ and $5f^{n-1}6d(t_{2g})^1$ states have been validated by the good agreement found between the theoretical and experimental $5f \leftrightarrow 6d(t_{2g})$ band profiles corresponding to the totally symmetric a_{1g} vibrational progression built on a single electronic origin[19,22,23] and on multiple electronic origins.[21,24] The same trend in bond lengths has been found in lanthanide ion impurities in chloride hosts like $Cs_2NaYCl_6:Ce^{3+}$ and $Cs_2NaYCl_6:Pr^{3+}$,[25] and on U^{4+}-doped fluoride hosts.[26]

The objective of this paper is to provide an explanation of the unexpected bond distance trend in the configurations $5f^n$ and $5f^{n-1}6d^1$. We do it by means of a quantum chemical analysis of the chemical bond in the $(CeCl_6)^{3-}$ and $(PrCl_6)^{3-}$ clusters embedded in Cs_2NaYCl_6 and in the $(PaCl_6)^{2-}$ and $(UCl_6)^{2-}$ clusters embedded in Cs_2ZrCl_6. In particular, the effects of ionic bond, charge transfer, and covalency on the bond distances calculated with complete active space self-consistent-field (CASSCF) wave functions[27] and a spin–free embedded cluster Hamiltonian[28,29] have been analyzed using the constrained space orbital variation (CSOV) method.[30,31] Spin–orbit coupling effects and dynamic electron correlation effects, which are neccessary for detailed spectroscopic studies on these materials, have been shown not to be responsible for the bond distance trend under study.[19–21] The details of the CSOV calculations are presented in Sec. II, the results are discussed in Sec. III, and the conclusions appear in Sec. IV.

II. DETAILS OF THE CALCULATIONS

A. $(LnCl_6)^{3-}$ and $(AnCl_6)^{2-}$ embedded clusters

We performed embedded cluster calculations on $(CeCl_6)^{3-}$ and $(PrCl_6)^{3-}$ embedded in Cs_2NaYCl_6 and on $(PaCl_6)^{2-}$ and $(UCl_6)^{2-}$ embedded in Cs_2ZrCl_6. Previous theoretical studies on these systems have established the effects of spin–orbit coupling and dynamic electron correlation on their structural parameters and spectroscopy, as well as reasonable methodological choices regarding core/valence partitions, valence basis sets, and active orbital spaces for multiconfigurational expansions.[19–21,25] Here, we have not chosen the theoretical level which is adequate for a correct description of the spectroscopy and the absolute values of the structural parameters, which requires spin–orbit calculations with dynamic correlation. Instead, we have used a simpler theoretical level: CASSCF wave functions and a spin–free embedded cluster Hamiltonian. This level is sufficient for a correct description of the bond distance trends in the f^n, $f^{n-1}d(t_{2g})^1$, and $f^{n-1}d(e_g)^1$ manifolds[19–21] and adequate for the analysis of the basic bonding interactions responsible for the unexpected bond distance shifts between manifolds. The CASSCF wave functions include all possible configurations where the open-shell electrons [one in $(CeCl_6)^{3-}$ and $(PaCl_6)^{2-}$; two in $(PrCl_6)^{3-}$ and $(UCl_6)^{2-}$] occupy the 12 molecular orbitals with main character Ln $4f$ (An $5f$) and Ln $5d$ (An $6d$): a_{2u}, t_{2u}, t_{1u}, t_{2g}, and e_g. (Note that we will refer to the molecular orbitals by their main atomic orbital character all throughout this paper.) We have performed the CASSCF calculations on electronic states of each cluster which are representative of the three different manifolds. They are the $4f^1-{}^2A_{2u}$, $5d(t_{2g})^1-{}^2T_{2g}$, and $5d(e_g)^1-{}^2E_g$ states of $(CeCl_6)^{3-}$, and the $4f^2-1{}^3T_{1g}$, $4f^15d(t_{2g})^1-1{}^3T_{1u}$, and $4f^15d(e_g)^1-4{}^3T_{1u}$ states of $(PrCl_6)^{3-}$, as well as the corresponding ones of $(PaCl_6)^{2-}$ and $(UCl_6)^{2-}$ (with the obvious difference of the involved orbitals being $5f$ and $6d$ instead).

We have used *ab initio* model potentials (AIMPs) both as embedding potentials[28,29] and as relativistic effective core potentials.[29,32,33] For Ce^{3+} and Pr^{3+} we used the [Kr,$4d$] core spin free relativistic Cowan–Griffin–Wood–Boring AIMP and ($14s10p9d8f$) valence basis sets from Ref. 33 contracted as [$6s5p5d4d$]. For Pa^{4+} and U^{4+} we used the [Xe,$4f$,$5d$] core spin free relativistic Cowan–Griffin–Wood–Boring AIMP and ($14s10p11d9f$) valence basis sets from Refs. 19 and 20, respectively, contracted as [$6s5p5d4f$]. For chlorine, we used the [Ne] core relativistic Cowan–Griffin–Wood–Boring AIMP and valence basis set ($7s6p$) of Ref. 34 augmented by $1p$ diffuse function for anions,[35] contracted as [$3s4p$]. Polarization functions were neither used on the Ln (An) nor on the Cl basis sets. For $(LnCl_6)^{3-}$ clusters, which are embedded in the Cs_2NaYCl_6 elpasolite, the ($7s4p$) basis set of the second neighbor Na^+ ions from Ref. 36 was also included, contracted as [$1s1p$]; these so-called second-neighbor basis functions are needed to fulfill strong orthogonality conditions with the lattice ion wave functions on crystals like the Cs_2NaYCl_6 elpasolite where Na^+ ions occur at near (100) sites; they are not necessary on crystals like Cs_2ZrCl_6 where the equivalent sites are vacant.[29,37] The embedding potentials used to describe the interactions between the $(LnCl_6)^{3-}$ and $(AnCl_6)^{2-}$ defect clusters and their Cs_2NaYCl_6 and Cs_2ZrCl_6 crystalline environment were obtained in Refs. 36 and 19, respectively; they have been used to study the structure and spectroscopy of transition metal ion impurities[36,38] and lanthanide and actinide ion impurities.[19–21,25] The core and embedding AIMP data can be found in Ref. 39. All the calculations have been performed with the MOLCAS package.[40]

B. Constrained space orbital variation analysis

The unconstrained CASSCF calculations will be called covalent calculations from now on, because they include all covalent effects other than dynamic correlation. In these, the molecular orbitals are free to vary, within the space spanned by the basis set, in order to minimize the CASSCF energy at each value of the Ln–Cl (An–Cl) distance. According to the CSOV method, a detailed, quantitative analysis of the bonding interactions can be made by constraining the variation of the molecular orbitals in controlled steps, where only specific orbital rotations are allowed.[30,31] Here, we perform four

CSOV steps which are described below. We calculate the equilibrium distances of all the states indicated in the previous Section in each CSOV step. (We do this with a polinomial fitting of four or five points of the corresponding potential energy curve, which gives bond distances stable in ± 0.001 Å aproximately.)

For the sake of clarity, we will refer only to the Ln cases from now on, meaning that, unless specified, the same calculation or discussion applies to the corresponding An case after obvious changes are made, i.e., $5f$ by $4f$, $6d$ by $5d$, An^{4+} by Ln^{3+}, $(PaCl_6)^{2-}$ by $(CeCl_6)^{3-}$, $(UCl_6)^{2-}$ by $(PrCl_6)^{3-}$, etc.

1. Step 0: symmetry adapted atomic orbitals

This is a preparatory step which provides symmetry adapted atomic orbitals to be used as initial guess for the first CSOV step. In it, CASSCF calculations are performed on the octahedral $(LnCl_6)^{3-}$ clusters *in vacuo*, with an infinite Ln–Cl distance (1000 a.u. in practice). The electronic configurations correspond to the formal oxidation states: Ln^{3+} and Cl^-. The molecular orbitals come out to be clean symmetry adapted atomic orbitals, whithout any mixture between Ln and Cl basis set functions.

2. Step 1: ionic model

At this step, CASSCF calculations are performed on the $(LnCl_6)^{3-}$ clusters embedded in the host, using the symmetry adapted atomic orbitals from step 0 as starting orbitals. The variations of the molecular orbitals are constrained as follows: Rotations between the Ln occupied and virtual orbitals are allowed; rotations between the Cl occupied and virtual orbitals are allowed; rotations between Ln orbitals and Cl orbitals are not allowed. Under these conditions, the final orbitals of step 1 are atomic like orthogonal orbitals resulting from the relaxation and polarization of the ionic Ln^{3+} and Cl^- segments under the effects of one another in the presence of the host, but excluding charge transfer from and to any of the two ionic segments, as well as covalency. This step corresponds to an ionic model.

The orbitals of this step will be referred to as ionic orbitals from now on and they are used as input orbitals for each of the next CSOV steps. Accordingly, any orbitals which are not allowed to rotate in a subsequent CSOV step will be kept frozen in their ionic model description. We have designed the next CSOV steps so that sequential orbital mixing from the ionic model to the final covalent model is allowed to progress inwards, as indicated by the radial extent of the occupied ionic orbitals: $5d > 5sp > 4f$. In all cases, comparison of the results of a given CSOV step with the previous one gives direct information on the role of particular orbitals.

3. Step 2: frozen 4f5sp

Now, starting with the ionic orbitals, rotations are allowed between Cl-occupied, Cl-virtual, Ln $5d$, and Ln-virtual orbitals. Only Ln $4f5sp$ ionic orbitals are kept frozen. Comparing this step with step 1 gives information relative to charge transfer from the ligands to Ln orbitals other than Ln $4f$, plus orbital mixing between Cl orbitals and Ln $5d$ orbitals in the $4f^n5d^1$ states.

4. Step 3: frozen 4f

Starting from the ionic molecular orbitals, this step includes additional orbital rotation freedom over step 2, since the occupied $5sp$ orbitals are also released and are free to rotate with Ln $5d$ and Ln-virtual orbitals, as well as with all Cl orbitals. Then, the role of Ln $5sp$ orbitals on bonding results from comparing this step and step 2.

5. Step 4: covalent model

The CASSCF calculations are now performed without any restrictions, as mentioned above. Comparison of this step and step 3 reveals the role of $4f$ orbitals on nonionic bonding, mainly through ligand to Ln $4f$ charge transfer because the covalent interactions between Ln $4f$ and Cl are shielded by the presence of the outermost Ln $5sp$ filled shell.

III. RESULTS

The results of the CSOV analysis of bonding interactions performed on representative states of the three configurations f^n, $f^{n-1}d(t_{2g})^1$, and $f^{n-1}d(e_g)^1$, of the four representative systems are presented and discussed here. The numerical results appear in Table I. Bonding effects on bond lengths are shown in Fig. 1 and on bond length difference with respect to the f^n configuration in Fig. 2. We have also included in Table I and Figs. 1 and 2 the bond distances calculated from the potential energy curves of the $f^{n-1}d^1$ baricenters, defined as

$$E[f^{n-1}d^1] = \{6E[f^{n-1}d(t_{2g})^1] + 4E[f^{n-1}d(e_g)^1]\}/10.$$

Although the $f^{n-1}d^1$ baricenters are not real states, they are convenient as a reference for discussion because they correspond to removal of d ligand field splitting effects. We will first comment on the results of the ionic and covalent models; later, we will discuss the results of the CSOV analysis of bonding interactions from one limit to the other.

In the ionic model, the four systems under study have a larger bond distance in the $f^{n-1}d^1$ baricenter configuration than in the f^n configuration (0.003 and 0.004 Å larger in the Ln^{3+} impurities and 0.024 Å larger in the An^{4+} impurities). These results qualitatively agree with the extended assumption on the bond distances in f^n and $f^{n-1}d^1$ configurations. However, they do not support any quantitative or semiquantitative interpretation or prediction based on the radial extent of the $4f$ and $5d$ shells of the free ions, which exhibit much larger differences, as it is shown in Table II (0.66 Å in Ln^{3+} and 0.52 Å in An^{4+}). The results of the covalent model show that covalency lowers all the bond distances (see Fig. 1), being the covalent effects more important in the $5d$ electrons than in the $4f$ electrons, and in An than in Ln, as illustrated by the covalent effects on the baricenter offset $R_e[f^{n-1}d^1] - R_e[f^n]$ [-0.007 Å (Ce^{3+}), -0.009 Å (Pr^{3+}), -0.012 Å (Pa^{4+}), and -0.018 Å (U^{3+})], leading to bond lengths which are very similar in the f^n configurations and in the $f^{n-1}d^1$ baricenter configurations in the four systems: slightly larger in the f^n configurations of Ln^{3+} im-

TABLE I. CSOV analysis of the Ln–Cl and An–Cl bond distances R_e (in Å) of $Cs_2NaYCl_6:(CeCl_6)^{3-}$, $Cs_2NaYCl_6:(PrCl_6)^{3-}$, $Cs_2ZrCl_6:(PaCl_6)^{2-}$, and $Cs_2ZrCl_6:(UCl_6)^{2-}$, in representative states of the configurations f^n, $f^{n-1}d(t_{2g})^1$, and $f^{n-1}d(e_g)^1$. The results of spin–free relativistic embedded cluster CASSCF calculations are presented. Bond distances in the baricenters of the two last configurations are shown under the labels d^1 and f^1d^1.

		$(CeCl_6)^{3-}$					
Step	model	$4f^1$	$5d^1$	$5d^1-4f^1$	$5d(t_{2g})^1$	$5d(e_g)^1$	$5d(t_{2g})^1-4f^1$
1	Ionic	2.846	2.849	+0.003	2.835	2.868	−0.011
2	Frozen Ce $4f5sp$	2.771	2.769	−0.002	2.746	2.801	−0.025
3	Frozen Ce $4f$	2.769	2.766	−0.003	2.744	2.798	−0.025
4	Covalent	2.749	2.745	−0.004	2.720	2.780	−0.029
	Covalent–ionic	−0.097	−0.104	−0.007	−0.115	−0.088	−0.018
		$(PrCl_6)^{3-}$					
		$4f^2$	$4f^15d^1$	$4f^15d^1-4f^2$	$4f^15d(t_{2g})^1$	$4f^15d(e_g)^1$	$4f^15d(t_{2g})^1-4f^2$
1	Ionic	2.830	2.834	+0.004	2.822	2.852	−0.008
2	Frozen Pr $4f5sp$	2.752	2.751	−0.001	2.729	2.783	−0.023
3	Frozen Pr $4f$	2.749	2.748	−0.001	2.726	2.780	−0.023
4	Covalent	2.736	2.731	−0.005	2.706	2.766	−0.030
	Covalent–ionic	−0.094	−0.103	−0.009	−0.115	−0.086	−0.022
		$(PaCl_6)^{2-}$					
		$5f^1$	$6d^1$	$6d^1-5f^1$	$6d(t_{2g})^1$	$6d(e_g)^1$	$6d(t_{2g})^1-5f^1$
1	Ionic	2.851	2.875	+0.024	2.859	2.898	+0.008
2	Frozen Pa $5f6sp$	2.747	2.762	+0.015	2.737	2.800	−0.010
3	Frozen Pa $5f$	2.742	2.759	+0.017	2.734	2.796	−0.008
4	Covalent	2.688	2.700	+0.012	2.671	2.743	−0.017
	Covalent–ionic	−0.163	−0.175	−0.012	−0.188	−0.155	−0.025
		$(UCl_6)^{2-}$					
		$5f^2$	$5f^16d^1$	$5f^16d^1-5f^2$	$5f^16d(t_{2g})^1$	$5f^16d(e_g)^1$	$5f^16d(t_{2g})^1-5f^2$
1	Ionic	2.816	2.840	+0.024	2.825	2.862	+0.009
2	Frozen U $5f6sp$	2.727	2.743	+0.016	2.719	2.778	−0.008
3	Frozen U $5f$	2.723	2.740	+0.017	2.716	2.775	−0.007
4	Covalent	2.677	2.683	+0.006	2.653	2.727	−0.024
	Covalent–ionic	−0.139	−0.157	−0.018	−0.172	−0.135	−0.033

purities (0.004 and 0.005 Å) and slightly larger in the $f^{n-1}d^1$ baricenter configurations of An^{4+} impurities (0.012 and 0.006 Å). All this seems to support a simple model, similar to the superconfiguration model proposed by Field for lanthanide monoxides,[41] according to which the bond distance in the $4f^n$ configuration is basically determined by the interaction of the ligands with the outer Ln $5p^6$ closed shell rather than with the inner Ln $4f^n$ open shell, which is very efficiently screened from the ligands by the Ln $5p^6$ barrier, whereas the bond distance in the $4f^{n-1}5d^1$ configuration depends on the interactions of the ligands with the $5d^1$ electron, which is now outside the Ln $5p^6$ barrier, and with the Ln $5p^6$ closed shell, with additional attractive effects coming from the inner $4f$ hole left behind by the promoted electron, via charge transfer. According to this simplified model, the difference between the bond distance in the $4f^{n-1}5d^1$ baricenter configuration and the $4f^n$ configuration should be slightly smaller than $\langle r\rangle_{5p^65d^1}-\langle r\rangle_{5p}$, with $\langle r\rangle_{5p^65d^1}=[6\langle r\rangle_{5p}+\langle r\rangle_{5d}]/7$ and, so, much smaller than expected from the comparisons of the radial extents of the $5d$ and $4f$ free-ion orbitals, which is what is observed: they are some 0.02 Å smaller than the $\langle r\rangle_{5p^65d^1}-\langle r\rangle_{5p}$ values (the same is true for the actinoids, see Fig. 2 and Tables I and II). Also in agreement with this view is the fact that the difference between $f^{n-1}d^1$ and f^n bond distances is approximately 0.01 Å larger in actinoids than in lanthanoids, as it is the difference between the mentioned radial expected values (Fig. 2).

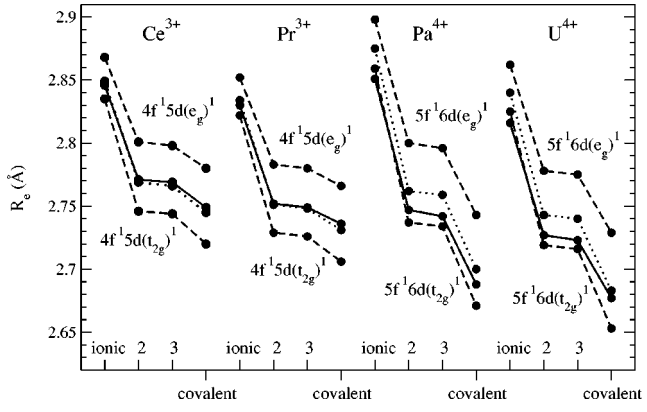

FIG. 1. CSOV analysis of the Ln–Cl and An–Cl bond distances R_e of Ce^{3+}-, Pr^{3+}-doped Cs_2NaYCl_6, and Pa^{4+}-, U^{4+}-doped Cs_2ZrCl_6 crystals in representative states of the configurations f^n (solid line), $f^{n-1}d(t_{2g})^1$, and $f^{n-1}d(e_{2g})^1$ (dashed lines). The results of the $f^{n-1}d^1$ baricenters (dotted lines) are also shown. The CSOV results of steps 1, 2, 3, and 4 (see Sec. II B for details) are labeled here "ionic," "2," "3," and "covalent."

Ligand field effects and the facts supporting this simple

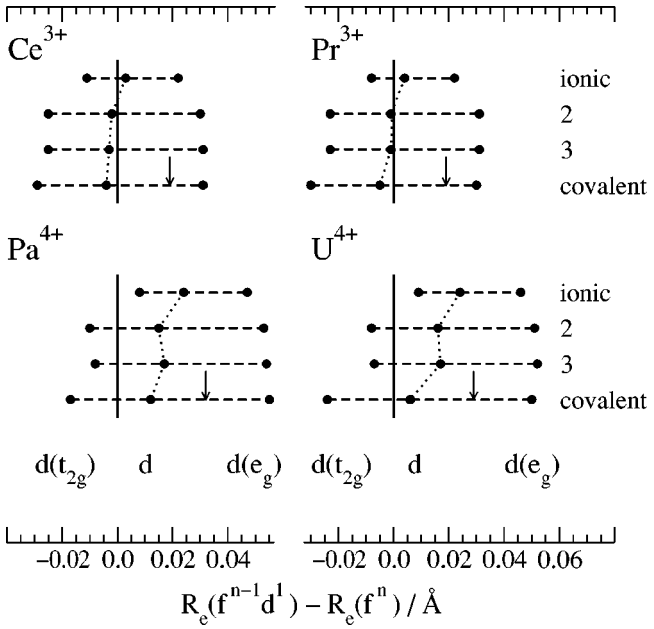

FIG. 2. Offset of the equilibrium distances R_e of the $f^{n-1}d(t_{2g})^1$ and $f^{n-1}d(e_{2g})^1$ states, and their baricenter $f^{n-1}d^1$, relative to the f^n ground state values, for Ce^{3+}-, Pr^{3+}-doped Cs_2NaYCl_6 and Pa^{4+}-, U^{4+}-doped Cs_2ZrCl_6. See captions of Table I and Fig. 1 for notation (ionic, 2, 3, covalent). Estimation of $R_e[f^{n-1}d^1]-R_e[f^n]$ shifts with $\langle r\rangle_{5p^65d^1}-\langle r\rangle_{5p}$ and $\langle r\rangle_{6p^66d^1}-\langle r\rangle_{6p}$, are indicated with vertical arrows.

model, namely, that all the f open-shell electrons are protected from ligand effects in the f^n and $f^{n-1}d^1$ configurations, but the d electron is exposed to them in the $f^{n-1}d^1$ configuration, are resposible for the observed grouping of bond distances according to their configurations f^n, $f^{n-1}d(t_{2g})^1$, and $f^{n-1}d(e_g)^1$.[20,21] In effect, the ligand field effects on the R_e values of all the electronic states belonging to the f^n configuration are very small, so that all of them show very similar bond length, whereas the large ligand field splitting of the d orbitals makes the $d(t_{2g})$ much more stable than the $d(e_g)$, so that the $f^{n-1}d(t_{2g})^1$ states have a bond distance which is much shorter than in the $f^{n-1}d(e_g)^1$ states. In the ionic model, the $d(t_{2g})$ stabilization lowers the bond length of the $f^{n-1}d(t_{2g})^1$ states with respect to the $f^{n-1}d^1$ baricenter configuration by amounts [0.014 Å (Ce^{3+}), 0.012 Å (Pr^{3+}), 0.016 Å (Pa^{4+}), and 0.015 Å (U^{3+})] which are sufficient to make the $f^{n-1}d(t_{2g})^1$ bond lengths to be shorter than the f^n ones in the Ln^{3+} impurities, where f^n and $f^{n-1}d^1$ bond lengths were very close, but not in An^{4+} impurities, where the differences were larger. Covalent effects mean an additional and large $d(t_{2g})$ stabilization, bringing the $f^{n-1}d(t_{2g})^1$ bond lengths clearly below the f^n ones in all cases. It is accompanied by a significant $d(e_g)$ unstabilization, meaning an increase of the effective ligand fields. The final bond length sequence of the covalent calculations is $R_e[f^{n-1}d(t_{2g})^1]<R_e[f^n]<R_e[f^{n-1}d(e_g)^1]$ in all cases (see Table I and Fig 2).

CSOV steps 2 and 3 allow one to perform an analysis of specific covalent effects on bond lengths and bond length offsets. Ligand to Ln charge transfer has a major impact on them. The effects of charge transfer from ligand (mainly Cl $3p$) to Ln orbitals other than $4f$, together with Ln $5d$ orbital mixing, is obtained comparing step 1 (ionic) with step 2: -0.005 Å in Ln^{3+} and $-0.008\sim-0.009$ Å in An^{4+} for $R_e[f^{n-1}d^1]-R_e[f^n]$, and $-0.014\sim-0.015$ Å in Ln^{3+} and $-0.017\sim-0.018$ Å in An^{4+} for $R_e[f^{n-1}d(t_{2g})^1]-R_e[f^n]$. [Further analysis of these contributions requires an intermediate frozen-$4f5spd$ CSOV calculation which would provide specific information on the effects of Ln $5d$ participation on bonding. For this calculation to be made, the Ln $5d$ orbitals must be identified among the virtual orbitals of the f^n state in the ionic calculations (CSOV step 1) in order to freeze them. This was possible in $(CeCl_6)^{3-}$ and $(PaCl_6)^{2-}$; in $(PrCl_6)^{3-}$ and $(UCl_6)^{2-}$ the mixture with correlating orbitals was high and the identification was not clear. The results showed that in $(CeCl_6)^{3-}$ the effect is dominated by Ln $5d$ participation on bonding (via charge transfer plus orbital mixing) which amounts -0.004 Å of the -0.005 Å effect on $R_e[f^{n-1}d^1]-R_e[f^n]$, and -0.012 Å of the -0.014 Å effect on $R_e[f^{n-1}d(t_{2g})^1]-R_e[f^n]$, whereas in $(PaCl_6)^{2-}$ a similar contribution of the Ln $5d$ participation on bonding and of charge transfer from ligands to Ln virtual orbitals is observed, the former amounting -0.005 Å of the -0.009 Å effect on $R_e[f^{n-1}d^1]-R_e[f^n]$, and -0.007 Å of the -0.018 Å effect on $R_e[f^{n-1}d(t_{2g})^1]-R_e[f^n]$.

The effects of charge transfer from ligand to Ln $4f$ orbitals is obtained comparing step 4 (covalent) with step 3. They are also major effects. The $4f$ hole creted by the excitation of one electron to the $5d$ orbital, beyond the $5sp$

TABLE II. Mean values of r (in Å) of the free ions. Results of spin–free relativistic all-electron numerical Cowan–Griffin–Hartree–Fock calculations are presented.

		$\langle r\rangle_{4f}$	$\langle r\rangle_{5p}$	$\langle r\rangle_{5d}$	$\langle r\rangle_{5p^65d^1}$[a]	$\langle r\rangle_{5p^65d^1}-\langle r\rangle_{5p}$
Ce^{3+}	$4f^1-{}^2F$	0.540	0.913			
	$5d^1-{}^2D$		0.888	1.199	0.932	0.019
Pr^{3+}	$4f^2-{}^3H$	0.512	0.894			
	$4f^15d^1-{}^3H$	0.495	0.870	1.169	0.913	0.019
		$\langle r\rangle_{5f}$	$\langle r\rangle_{6p}$	$\langle r\rangle_{6d}$	$\langle r\rangle_{6p^66d^1}$[b]	$\langle r\rangle_{6p^66d^1}-\langle r\rangle_{6p}$
Pa^{4+}	$5f^1-{}^2F$	0.725	0.935			
	$6d^1-{}^2D$		0.920	1.247	0.967	0.032
U^{4+}	$5f^2-{}^3H$	0.690	0.915			
	$5f^16d^1-{}^3H$	0.687	0.900	1.207	0.944	0.029

[a]Defined as $\langle r\rangle_{5p^65d^1}=[6\langle r\rangle_{5p}+\langle r\rangle_{5d}]/7$.
[b]Defined as $\langle r\rangle_{6p^66d^1}=[6\langle r\rangle_{6p}+\langle r\rangle_{6d}]/7$.

closed shell, makes this charge transfer larger in the $f^{n-1}d^1$ states than in the f^n states, thus producing negative contributions to $R_e[f^{n-1}d^1]-R_e[f^n]$, again larger in An^{4+} than in Ln^{3+}: -0.001 Å (Ce^{3+}), -0.004 Å (Pr^{3+}), -0.005 Å (Pa^{4+}), and -0.011 Å (U^{3+}). The contributions to $R_e[f^{n-1}d(t_{2g})^1]-R_e[f^n]$ are -0.004 Å (Ce^{3+}), -0.007 Å (Pr^{3+}), -0.009 Å (Pa^{4+}), and -0.017 Å (U^{3+}). The ligand to Ln $4f$ charge transfer also increments the effective ligand field on the $5d$ orbitals.

Finally, the stiffness of the Ln $5p$ shell and its negligible impact on bond length offsets and almost negligible on bond lengths, is apparent when the CSOV results of steps 2 and 3 are compared.

IV. CONCLUSIONS

In this paper we have performed a CSOV analysis of bonding interactions in the four defect systems Ce^{3+}-doped and Pr^{3+}-doped Cs_2NaYCl_6, and Pa^{4+}-doped and U^{4+}-doped Cs_2ZrCl_6, which are responsible for the grouping of electronic states according to their structural properties in: $f^{n-1}d(t_{2g})^1$, f^n, and $f^{n-1}d(e_g)^1$ states, as described in previous theoretical studies. The analysis has been performed on CASSCF wave functions of the $(CeCl_6)^{3-}$ and $(PrCl_6)^{3-}$ clusters embedded in Cs_2NaYCl_6 and the $(PaCl_6)^{2-}$ and $(UCl_6)^{2-}$ clusters embedded in Cs_2ZrCl_6, using a spin–free relativistic Cowan–Griffin–Wood–Boring AIMP Hamiltonian. It has revealed the quantitative effects on bond lengths and bond length offsets of ligand to Ln (An) charge transfer, which has suggested a simple and novel interpretative model. According to it, the appearence of three basic bond lengths and their sequence is due mainly to the following: The inner Ln $4f^n$ (An $5f^n$) open-shell electrons are all shielded from the ligands by the outer Ln $5p^6$ (An $6p^6$) closed-shell electrons, whose interaction with the ligands determines the bond distance in states of the f^n configuration. Instead, in $f^{n-1}d^1$ configurations, one electron has crossed the $5p^6$ ($6p^6$) barrier and is exposed to covalent interactions with the ligands, leaving a $4f$ ($5f$) whole behind, both effects leading to a shortening of the bond length. Finally, a large $5d(t_{2g})-5d(e_g)$ [$6d(t_{2g})-6d(e_g)$] ligand field splitting, which is enhanced by covalency, lowers the $f^{n-1}d(t_{2g})^1$ bond lengths clearly below the f^n ones, and raises the $f^{n-1}d(e_g)^1$ ones clearly above them.

ACKNOWLEDGMENT

This work was partly supported by a grant from Ministerio de Ciencia y Tecnología, Spain (Dirección General de Investigación, Grant No. BQU2002-01316).

[1] J. Ehrlich, P. F. Moulton, and R. M. Osgood, Jr., Opt. Lett. **4**, 117 (1979).
[2] M. Nikl, Phys. Status Solidi A **178**, 595 (2000).
[3] V. N. Makhov, N. M. Khaidukov, N. Y. Kirikova, M. Kirm, J. C. Krupa, T. V. Ouvarova, and G. Zimmerer, J. Lumin. **87**, 1005 (2000).
[4] N. M. Khaidukov, M. Kirm, S. K. Lam, D. Lo, V. N. Makhov, and G. Zimmerer, Opt. Commun. **184**, 183 (2000).
[5] P. A. Tanner, C. S. K. Mak, and M. D. Faucher, Chem. Phys. Lett. **343**, 309 (2001).
[6] I. Sokólska and S. Kück, Chem. Phys. **270**, 355 (2001).
[7] E. van der Kolk, P. Dorenbos, C. W. E. van Eijk, A. P. Vink, C. Fouassier, and F. Guillen, J. Lumin. **97**, 212 (2002).
[8] K. D. Oskam, A. J. Houtepen, and A. Meijerink, J. Lumin. **97**, 107 (2002).
[9] M. Laroche, M. Bettinelli, S. Girard, and R. Moncorgé, Chem. Phys. Lett. **311**, 167 (1999).
[10] R. Valiente, O. S. Wenger, and H. U. Güdel, Phys. Rev. B **63**, 165102 (2001).
[11] R. Balda, M. Voda, M. Al-Saleh, and J. Fernández, J. Lumin. **97**, 190 (2002).
[12] M. Illemassene, N. M. Edelstein, K. M. Murdoch, M. Karbowiak, R. Cavellec, and S. Hubert, J. Lumin. **86**, 45 (2000).
[13] P. J. Dereń, W. Stręk, E. Zych, and J. Drożdżyński, Chem. Phys. Lett. **332**, 308 (2000).
[14] S. V. Godbole, A. G. Page, Sangeeta, S. C. Sabharwal, J. Y. Gesland, and M. D. Sastry, J. Lumin. **93**, 213 (2001).
[15] N. Yu. Kirikova, M. Kirm, J. C. Krupa, V. N. Makhov, G. Zimmerer, and J. Y. Gesland, J. Lumin. **97**, 174 (2002).
[16] H. P. Andres, K. Krämer, and H. U. Güdel, Phys. Rev. B **54**, 3830 (1996).
[17] Y. Shen and K. L. Bray, Phys. Rev. B **58**, 11944 (1998).
[18] A. Meijerink and G. Blasse, J. Lumin. **43**, 283 (1989).
[19] L. Seijo and Z. Barandiarán, J. Chem. Phys. **115**, 5554 (2001).
[20] Z. Barandiarán and L. Seijo, J. Chem. Phys. **118**, 7439 (2003).
[21] L. Seijo and Z. Barandiarán, J. Chem. Phys. **118**, 5335 (2003).
[22] D. Piehler, W. K. Kot, and N. Edelstein, J. Chem. Phys. **94**, 942 (1991).
[23] N. Edelstein, W. K. Kot, and J. C. Krupa, J. Chem. Phys. **96**, 1 (1992).
[24] M. Karbowiak, E. Simoni, J. Drożdżyński, and S. Hubert, Acta Phys. Pol. A **90**, 367 (1996).
[25] L. Seijo, Z. Barandiarán, and B. Ordejón, Mol. Phys. **101**, 73 (2003).
[26] B. Ordejón, L. Seijo, and Z. Barandiarán (unpublished).
[27] B. O. Roos, P. R. Taylor, and P. E. M. Siegbahn, Chem. Phys. **48**, 157 (1980); P. E. M. Siegbahn, A. Heiberg, J. Almlöf, and B. O. Roos, J. Chem. Phys. **74**, 2384 (1981); P. Siegbahn, A. Heiberg, B. Roos, and B. Levy, Phys. Scr. **21**, 323 (1980).
[28] Z. Barandiarán and L. Seijo, J. Chem. Phys. **89**, 5739 (1988).
[29] L. Seijo and Z. Barandiarán, in *Computational Chemistry: Reviews of Current Trends*, edited by J. Leszczyński (World Scientific, Singapore, 1999), Vol. 4, p. 55.
[30] P. S. Bagus, K. Hermann, and C. W. Bauschlicher, J. Chem. Phys. **80**, 4378 (1984).
[31] C. W. Bauschlicher and P. S. Bagus, J. Chem. Phys. **81**, 5889 (1984).
[32] L. Seijo, J. Chem. Phys. **102**, 8078 (1995).
[33] L. Seijo, Z. Barandiarán, and E. Harguindey, J. Chem. Phys. **114**, 118 (2001).
[34] Z. Barandiarán and L. Seijo, Can. J. Chem. **70**, 409 (1992).
[35] T. H. Dunning and P. J. Hay, in *Modern Theoretical Chemistry*, edited by H. F. Schaefer III (Plenum, New York, 1977).
[36] A. Al-Abdalla, Z. Barandiarán, L. Seijo, and R. Lindh, J. Chem. Phys. **108**, 2005 (1998).
[37] J. L. Pascual, L. Seijo, and Z. Barandiarán, J. Chem. Phys. **98**, 9715 (1993).
[38] L. Seijo and Z. Barandiarán, J. Chem. Phys. **118**, 1921 (2003).
[39] Detailed core and embedding AIMP data libraries in electronic format are available from the authors upon request or directly at the address http://www.uam.es/quimica/aimp/Data/AIMPLibs.html. See also Ref. 40.
[40] K. Andersson *et al.*, MOLCAS Version 5 (Lund University, Sweden, 2000).
[41] R. W. Field, Ber. Bunsenges. Phys. Chem. **86**, 771 (1982).